Available online at www.sciencedirect.com
ScienceDirect
International Journal of Thermal Sciences 48 (2009) 573–582
International Journal of Thermal Sciences
www.elsevier.com/locate/ijts

Experimental and modelling study of superficial elastomer vulcanization by short wave infrared radiation

Pascal Le Bideau, Jean-Pierre Ploteau, Patrick Dutournié, Patrick Glouannec *

Laboratoire d'Etudes Thermiques, Energétiques et Environnement, Université de Bretagne Sud, Centre de recherche, B.P. 92116, Lorient Cedex, France

Received 4 December 2007; received in revised form 18 February 2008; accepted 23 March 2008

Available online 23 April 2008

Abstract

During the manufacturing of car body joints, many thermal processes are usually used to obtain the end product. Among these processes, infrared technology is widely employed, notably at the extruder outlet in order to quickly vulcanize superficially the elastomer. The extruded profile is next totally vulcanized during the process continuation. This superficial treatment is a major process step because it fixes the extruded product section and prevents thus shape deformations. A perfect knowledge of the infrared impact is necessary to provide a good quality of the end product. This paper deals with the study of superficial vulcanization of an EPDM-based rubber by infrared radiation. Thermo-physical properties and reaction kinetics were estimated by experimental measurements. A numerical model was developed to predict temperature and vulcanization profiles in the material thickness. In parallel, vulcanization tests were carried out on instrumented samples. The simulated temperature profiles were compared and validated with experimental ones and a new experimental methodology was implemented to determine and to validate the vulcanization profile in the sample thickness.

Keywords: Kinetic reaction; Rubber; Calorimetric analysis; IR heater; Thermo-physical properties

1. Introduction

Rubber materials are materials that are widely used in many industrial applications. For example, in the automotive industry, rubber gum is the main component of tires, low-pressure hoses or car body joints. Indeed, elastomers have several interesting qualities like an elastic behavior, a watertightness and damping qualities. To manufacture these products, uncured material is heated to a sufficient temperature in order to start the vulcanization reaction. Different heat transfer modes can be used to treat the material: convective (hot air tunnels, salt baths), conductive (hot molds) and radiative inputs (microwaves, infrared). Nevertheless, whatever the process, the final state of cure depends on cure time and temperature history. Moreover, depending on the degree of cure, mechanical properties and mechanical behavior of end products vary [1]. Therefore, to control mechanical behavior, a perfect knowledge of the vulcanization process is needed.

The main particularity of our work is to study rubber vulcanization under short-wave infrared radiation. Indeed, infrared technology can provide several advantages like a great quantity of energy transferred to the product without any medium, a reduction of cure time or an easy control of lamps power. For all these reasons, the infrared process enables to reduce cost production, to improve product quality and it is particularly adapted to superficial treatments [2,3]. Thus, in specific processes like the continuous production of automotive rubber seals, this technology is notably used at extruder outlet in order to vulcanize superficially the extruded profile. This operation allows to maintain a constant section product and to prevent geometric deformation during process continuation.

However, because of the low penetration depth of the infrared radiation and the low thermal conductivity of rubber, great temperature gradients can be generated inside the material. These temperature gradients create some vulcanization heterogeneities in the thickness wise called vulcanization profile.

* Corresponding author. Tel.: +33 (0) 2 97 87 45 11; fax: +33 (0) 2 97 45 0031.
E-mail address: patrick.glouannec@univ-ubs.fr (P. Glouannec).

1290-0729/$ – see front matter
doi:10.1016/j.ijthermalsci.2008.03.016

Nomenclature

Symbols

c_p	specific heat capacity	$J\,kg^{-1}\,K^{-1}$
h	heat transfer coefficient	$W\,m^{-2}\,K^{-1}$
E_{ir}	infrared radiation	$W\,m^{-2}$
E_a	activation energy	$J\,mol^{-1}$
ΔH	reaction enthalpy	$J\,kg^{-1}$
K_0	pre-exponential factor	s^{-1}
R	gas constant	$J\,mol^{-1}\,K^{-1}$
S_α	vulcanization heat source	$W\,m^{-3}$
T	temperature	K
t	time	s
X	state of vulcanization	

Greek letters

α	infrared absorptivity	
ε	emissivity	
k	thermal conductivity	$W\,m^{-1}\,K^{-1}$
ρ	density	$kg\,m^{-3}$
σ	Stefan–Boltzmann constant	$W\,m^{-2}\,K^{-4}$

Subscripts

a	ambient
e	sample bottom
end	end of test
exp	experimental measurements
res	residual
$\propto$	total
u	unvulcanized
v	vulcanized
w	wall

The objective of this work is to develop and validate a numerical model enabling the prediction of vulcanization profiles evolutions during the process of superficial vulcanization. A literature survey showed that several studies about the prediction of vulcanization evolution were performed. A great amount of these studies took an interest to rubber vulcanization in the instance of molding process [4–8] but only few works concerned the vulcanization of extruded profile by radiant technologies [2,9,10].

The distinctive feature of this work is that the present model integrates nonlinearity problems (great variation of thermo-physical properties) caused by dilatation phenomenon (non-compact blend). This geometric expansion is also considered in our model.

In this paper, an EPDM blend was studied. First, based on dynamic calorimetry measurements, a kinetic model was estimated and thermo-physical properties were measured. These properties were used to develop a thermal model representing the heat transfer, the dilatation and the vulcanization into a thin plate. Thereafter, to validate the studies, predicted temperature evolutions were compared with temperature measurements performed on an instrumented experimental pilot. Then, an experimental method enabling the validation of the vulcanization profile predicted by the model is presented.

2. Material

2.1. Blend studied

In this work, an ethylene-propylene-diene monomer (EPDM) rubber is studied. This blend prepared by an automotive manufacturer is a serial blend used to produce car body joints. It contains about 30 wt% EPDM gum, 40 wt% reinforcing agent (carbon black, chalk ...) and about 30 wt% of other components (oil, sulphur, activators, accelerators, antioxidant ...). The samples studied are prepared in a laboratory mixer.

2.2. Vulcanization kinetics

Kinetic characterization

A literature survey shows that several techniques are generally used to study vulcanization kinetics and to develop representative kinetic models. Among these methods, two main approaches are frequently applied to determine kinetic parameters: the mechanical approach and the calorimetric approaches in isothermal or non-isothermal modes [11–13]. In this paper, the kinetic study was performed by using these two approaches: torque measurements by rheometer and heat flow measurements by DSC in anisothermal mode.

A Mosanto Moving Die Rheometer was used to carry out torque measurements. These measurements were performed many times on some thin sheets of rubber (2 mm thickness) at different temperatures (160, 170, 180 and 190 °C) in constant test condition (±0.5° arc strain amplitude). Based on torque recordings, states of vulcanization evolutions can be deduced by the following formulation [14]:

$$X(t) = \frac{C_t - C_m}{C_M - C_m} \tag{1}$$

where C_t, C_m, C_M are respectively the torque value recorded at a time t, the minimum torque value and the maximum torque.

Fig. 1 shows the conversions evolutions estimated from these torques recordings. We can note that vulcanization reaction starts from the beginning of the test. A small induction period appears but it is less than 15 s. Consequently, in this paper, this induction period is neglected in the kinetic model. It can be seen that the cure rate rises with the temperature increase.

Several authors showed that cure rate and optimum cure time vary with the measurement approach [12–15]. In this study, calorimetric measurements were chosen to estimate kinetic parameters. Indeed, the vulcanization conditions in calorimetric approach are similar to our conditions (no mechanical shear force). Thus, several anisothermal DSC measurements were carried out at different heating rates and using the measure-

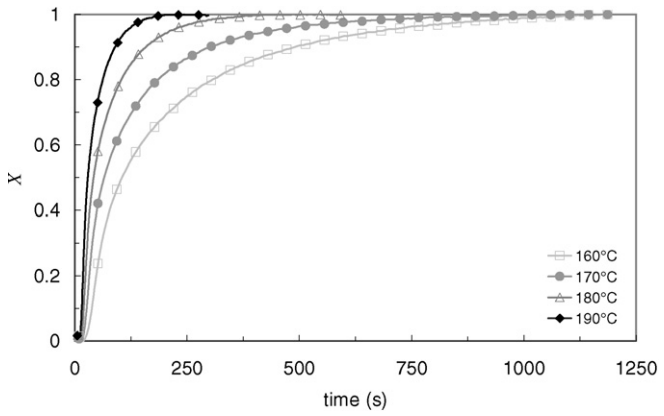

Fig. 1. States of vulcanization evolutions deduced from torque recordings at four temperatures.

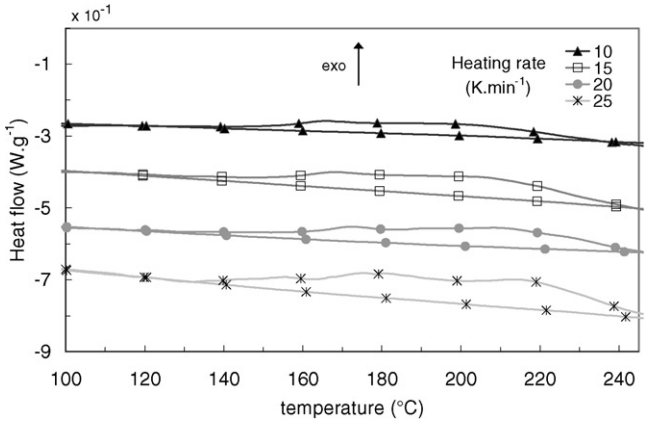

Fig. 2. Anisothermal DSC measurements at four heating rates.

ments of heat flow variations during the imposed temperature ramp, the state of vulcanization evolutions are calculated by:

$$X(t) = \frac{\int_0^t \frac{dh}{dt}\,dt}{\int_0^\infty \frac{dh}{dt}\,dt} = \frac{1}{\Delta H_\infty}\int_0^t \frac{dh}{dt}\,dt = \frac{\Delta H_t}{\Delta H_\infty} \tag{2}$$

where dh/dt is the heat flow measured by DSC, ΔH_t is the partial energy liberated until the moment t and ΔH_∞ is the total enthalpy of vulcanization reaction.

For a DSC run, about 20 mg of blend studied was placed in a non-hermetic aluminium pan and the scan was executed in helium atmosphere in a temperature range of 20 to 250 °C (DSC 2010 T.A. Instruments). Earlier, a thermogravimetric analysis was performed and showed that any mass losses should be considered in this temperature range. To confirm this result, the pans were weighed before and after the DSC run. Fig. 2 shows anisothermal DSC results performed at different heating rates 10, 15, 20 and 25 K min^{-1}. The exothermal reaction starts at about 120–130 °C and finishes at about 240 °C. Whatever the heating rate, we notice two exothermal reactions. The peak of the first one occurs for temperatures included between 170 and 180 °C according to the heating rate and the peak of the last one is visible between 200 and 220 °C. Finally, based on the DSC peak integration, average total enthalpy reaction is calculated (based on 11 DSC runs) and is estimated at 17.2 ± 0.9 J g^{-1}.

Using these DSC results experimental kinetic reactions can be estimated as follows:

$$\frac{dX}{dt} = \frac{1}{\Delta H_\infty}\frac{dh}{dt} \tag{3}$$

Kinetic model

According to the literature survey [16], the vulcanization reaction can be modeled as a temperature and conversion dependent functions:

$$\frac{\partial X}{\partial t} = F(T, X) \tag{4}$$

In many chemical reactions, the influence of the temperature and the state of vulcanization are separated [16], then the kinetic law is formulated as the product of two independent functions:

$$\frac{\partial X}{\partial t} = K(T)G(X) \tag{5}$$

To valid this hypothesis of separation of variables, it is necessary that, whatever the heating rate, the maxima of reaction rates are recorded at the same state of cure (for the first peak, $X_p \approx 0.25$ and for the second one, $X_p \approx 0.7$).

The temperature dependent function is expressed by an Arrhenius law:

$$K(T) = k_0 e^{-E_a/RT} \tag{6}$$

For the function $G(X)$, many equation forms are frequently employed: first order model [17], nth order model [18], autocatalytic model [19] or polynomial equation [20]. For this elastomer, two successive peaks are noticed (Fig. 2). Therefore, to model the vulcanization reaction, the global reaction is broken up in two autocatalytic reactions [21]. The formulation is as follows:

$$\frac{\partial X_i}{\partial t} = k_{0_i} e^{-E_{a_i}/RT} X^{m_i}(1-X)^{n_i}, \quad i = 1, 2 \tag{7}$$

Then, the total state of vulcanization is:

$$X = X_1 + X_2 \tag{8}$$

Activation energies are calculated using the Ozawa approach. Other parameters (pre-exponential factors and order reactions) are estimated by a least-square minimization method based on the Levenberg–Marquardt algorithm. At first, the parameters of the second reaction are identified using the late stage of global reaction rate. Indeed, for a state of vulcanization superior at 0.6, the contribution of reaction (1) is supposed to be null and, thus, the total conversion evolution is only induced by reaction (2). As soon as the kinetic parameters of reaction (2) are estimated, the contribution of reaction (2) is subtracted from the total reaction. The unknown parameters of reaction (1) are next identified. One example of identification results is shown in Fig. 3 for a temperature ramp imposed at 15 K/min from 20 to 270 °C. The global reaction rates and the contributions of reaction (1) and (2) are plotted versus time in Fig. 3(a). We can notice that reaction (2) is the preponderant reaction. The conversion evolution is represented in Fig. 3(b). We notice that

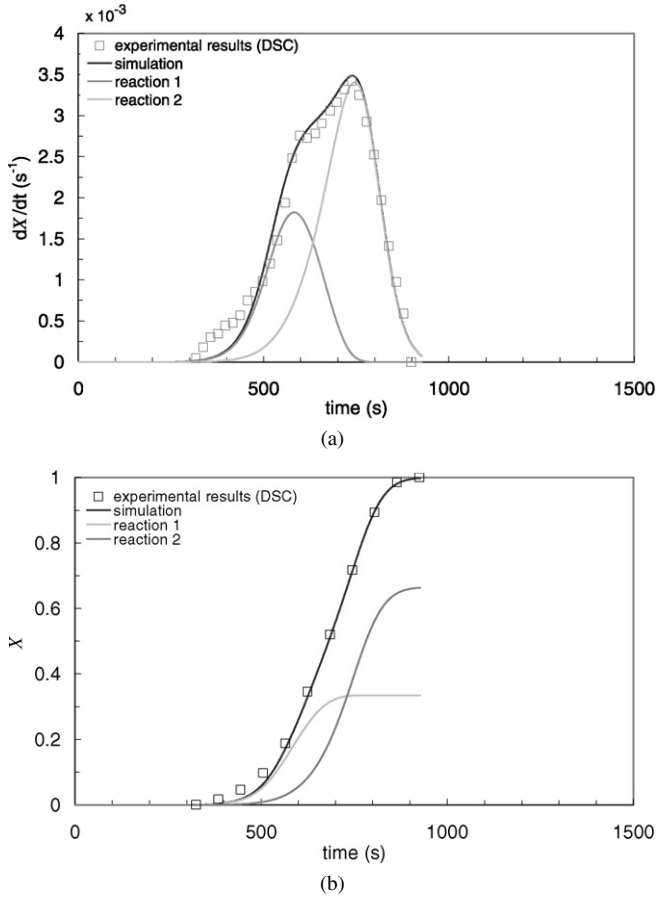

Fig. 3. Reaction rate and reaction contributions (kinetic reaction at 15 K/min).

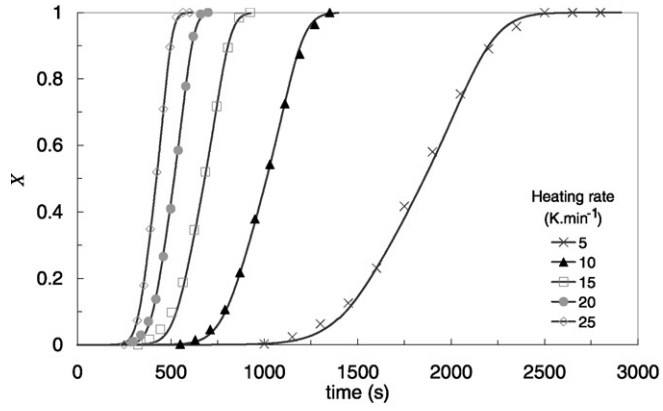

Fig. 4. States of vulcanization evolutions for different heating rates. Comparison between simulated results (solid lines) and DSC measurements (symbols).

the maximum conversion reached for reaction (1) is about 0.35 whereas it equals to 0.65 for reaction (2), which confirms the prevalence of the second reaction. Globally, the comparison of the total reactions measured with the global reactions simulated reveals a good agreement between the kinetic model and the experimental kinetic. Fig. 4 shows the evolutions of vulcanization conversions versus time obtained by DSC tests for several imposed temperature ramps. These evolutions are compared to the ones predicted by the kinetic model. Based on the observation of these results, we can assumed that the previously parameters set identified seems to be coherent in this heating rate range.

Table 1
Kinetic parameters obtained after identification

	K_0 (s^{-1})	E_a (kJ mol^{-1})	m	n
Reaction 1	2.7×10^{13}	128	0	6.25
Reaction 2	4.4×10^{11}	123	0	1.3

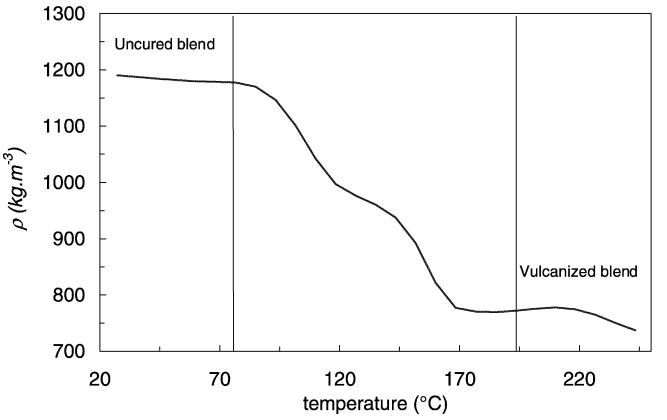

Fig. 5. Density evolutions during vulcanization DMA test.

The average kinetic parameter values originally from this identification step are listed in Table 1. We can note that the identified coefficients m_1 and m_2 equal zero, so the two reactions reduce to nth order reactions.

2.3. Thermo-physical properties

Density measurements were performed on an uncured blend and on a blend totally vulcanized at room temperature using a pycnometer. To estimate density evolutions with temperature and conversion evolution the sample deformation is expected to be isotropic and without mass losses. Then, thermal expansion coefficient $\Delta L/L0$ of the material was measured by Dynamic Mechanical Analyzer (Model 2980 of TA Instruments) in compression mode. A static force of 0.01 N is applied on a cylindrical sample, measuring initially 12.8 mm in diameter and 8 mm in height, and a slow temperature ramp is imposed (1 K/min) included between 20 and 250 °C. Fig. 5 shows the density evolution obtained. The density of uncured matter is approximately 1200 kg m^{-3} (value obtained by pycnometry method) and decreases until 740 kg m^{-3} for the matter totally cured (at 220 °C). Some analysis showed that density mainly varies with the state of vulcanization X and little varies with the temperature. Before the vulcanization starts ($T < 90$ °C), we note that the density is quasi-constant. At 30 °C, density equals 1190 kg m^{-3} and at 90 °C, density equals 1160 kg m^{-3}. A similar phenomenon is noticed when the blend is totally vulcanized. At 30 °C, density equals 730 kg m^{-3} (pycnometric method) and is equal to 735 kg m^{-3} (DMA method) at 250 °C. Whereas, we note that density greatly varies during the vulcanization step. To model this density variation, a polynomial equation based only on the state of vulcanization has been chosen (Fig. 5). The effect of temperature is not considered.

The specific heat evolutions of uncured and totally vulcanized samples were estimated by differential scanning calorime-

Table 2
Thermal properties of blend

	Unvulcanized	Vulcanized
Thermal conductivity ($W\,m^{-1}\,K^{-1}$)	0.315 (hot guarded method)	0.242 (Inverse method)
Specific heat ($J\,kg^{-1}\,K^{-1}$)	$3.11(T-273.15)+1409$ (DSC method)	$2.68(T-273.15)+1417$ (DSC method)
Density ($kg\,m^{-3}$)	1190 (pycnometry method)	740 (DMA method) 730 (pycnometry method) 755 (Inverse method)
Emissivity	0.85	
Absorptivity	0.6	

try (DSC 2010 T.A. Instruments). For each test, a small amount of matter (about 20 mg) is placed in non-hermetic aluminium pan. The DSC runs are performed in a temperature range of 20 to 250 °C at a heating rate of 20 K/min (limit at 100 °C for uncured rubber) under a helium atmosphere. A first run is conducted with an empty pan to obtain the baseline and the calibration was done with a standard sapphire sample. Based on these measurements, the temperature-dependent specific heat is next calculated for the uncured and vulcanized sample (Table 2). In order to considered specific heat variations with state of vulcanization, a mixing law [16] is established:

$$c_p(T, X) = Xc_{pv}(T) + (1 - X)c_{pu}(T) \tag{9}$$

The thermal conductivity of uncured sample was measured at three different temperatures (30–50–70 °C) by the guarded hot plate method. In the instance of the vulcanized matter, the thermal conductivity was estimated by a transient method based on the work of K.J. Dowding et al. [22] in the range 30 to 160 °C. This method, which needs an experimental setup coupled with an inverse method measures simultaneous temperature dependent thermal conductivity and volumetric heat capacity. These measurements showed that thermal conductivities little vary with temperature but depend of states of vulcanization.

The thermo-optical properties, average infrared absorption coefficient and emissivity were evaluated by Fourier Transform Infrared Spectroscopy (FTIR) using an Attenuated Total Reflectance (ATR) module. The elastomer sample was considered as a semi gray body (diffuse reflection and emission). Next, based on the reflectance measurements and the body emittance, the optical properties were estimated in first approximation [23,24].

3. Study of infrared curing

3.1. Phenomena description

During the superficial treatment by infrared radiation, different thermal phenomena are present and have to be considered in this study. When the sample is exposed to a great infrared radiation (several $kW\,m^{-2}$), its surface temperature quickly rises and exchanges heat by convection and long-wave radiation (Fig. 6). Because of the low penetration depth of infrared radiation into matter and the low thermal conductivity of rubber, great temperature gradients are generated inside material. These thermal

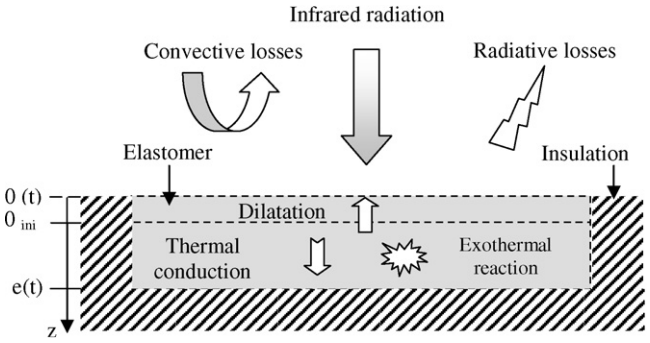

Fig. 6. Thermal phenomena.

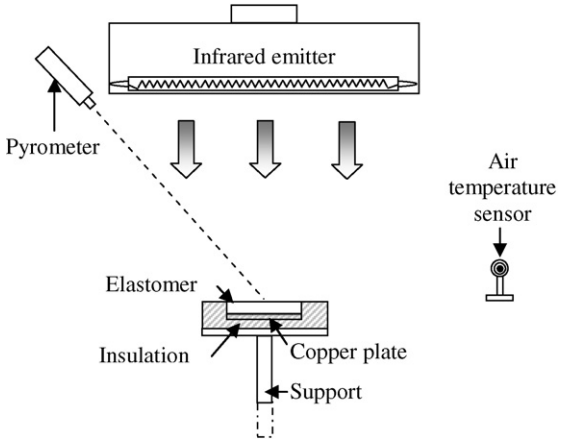

Fig. 7. Experimental setup.

gradients induce vulcanization profile in the thickness and consequently generate a sample dilatation (geometric deformation) which is taken into account in the numerical model. In this work, a plane plate configuration with thermally insulated side faces is considered in order to suppose an one-dimensional heat transfer.

3.2. Experimental setup

The experimental setup which was developed in our laboratory (Fig. 7) is mainly composed of a radiant heat source. This radiant heat source is equipped with three short-wave infrared lamps (2 kW each). Each lamp is fitted out with a parabolic reflector to assure a homogeneous radiation area. A power controller unit regulates the dissipated energy. The last one cited operates in syncopated wave train is itself piloted by an input voltage (0–10 V). The elastomer sample (Fig. 8) previously instrumented in temperature sensors and insulated is positioned under the emitter in a mobile support which enables the control of the heat source-sample distance.

The sample dimensions are 60 mm to-side and about 8 mm thick. An optical pyrometer measures surface temperature and each sample is instrumented with K-type thermocouples (welding diameter: 300 μm). These ones embedded into matter are placed parallel to the isotherms (Fig. 8). A copper plate of 0.5 mm is intercalated between the bottom of the sample and the thermal insulation in order to homogenize bottom temperature.

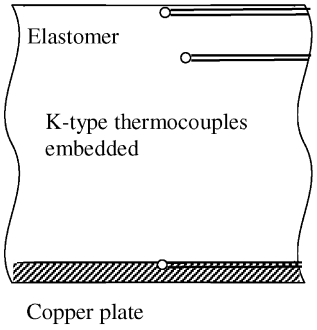

Fig. 8. Instrumentation sample representation.

A thermocouple embedded in this plate measure the temperature. Another temperature sensor, protected against the incident radiation by a radiation shield, records the air temperature.

All this sensors are connected to a data acquisition system (10 acquisitions per second). Before each test, the incident heat flux is measured with a flux meter previously developed in our laboratory [25].

For the experimental tests, the samples were first positioned in the support and the infrared lamps were switched on. During about three hundred seconds, period to reach a constant incident radiation (emitter transient state), a radiant shield was placed between the emitter and the sample. Next, the plate was removed. At the end of heating period, the shield was replaced again in order to prevent radiative exchanges between the emitter and the sample.

3.3. Thermal model

From this thermal phenomena analysis, a one-dimensional knowledge model is developed to represent the heat transfers during the vulcanization process. Into matter, the governing equation is the following:

$$\rho c_p(T,X)\frac{\partial T}{\partial t} = \frac{\partial}{\partial z}\left(k(X)\frac{\partial T}{\partial z}\right) + S_X(T,X) \tag{10}$$

In this governing equation, the source term S_X represents the energy dissipated during the vulcanization reaction:

$$S_X(T,X) = \rho(T,X)\Delta H_\infty \frac{\partial X}{\partial t} \tag{11}$$

The upper face of the sample ($z = 0$) is exposed to the short infrared radiation, convective and long infrared radiation (Fig. 6). At the sample bottom ($z = e$), a Dirichlet condition is imposed and equals to the temperature measured at the sample bottom.

So, the boundary conditions are defined as follow:

At $z = 0$ and $t < t_r$

$$-k\left(\frac{\partial T}{\partial z}\right)_0 = h(T - T_a) + \frac{\varepsilon\sigma F_{0-w}(T^4 - T_w^4)}{(1-\varepsilon)F_{0-w} + \varepsilon} + \alpha E_{\text{ir}} \tag{12}$$

At $z = 0$ and $t > t_r$

$$-k\left(\frac{\partial T}{\partial z}\right)_0 = h(T - T_a) + \varepsilon\sigma F_{0-w}\left(T^4 - T_w^4\right)$$

At $z = e$

$$T(z = e, t) = T_{\exp}(z = e, t) \tag{13}$$

In Eqs. (12), t_r is the time during which the sample is exposed to the short-wave infrared radiation. For the radiant exchanges between the emitter and the sample surface, the incident heat flux E_{ir} is measured by a fluxmeter [25].

For the long wave radiation a view factor F_{0-w} is introduced. F_{0-w} is equal to 0.82 during the short-wave infrared radiation [26]. It is taken equal to 1 during the cooling period (the radiant shield placed between the emitter and the sample is supposed at the environment temperature).

The convective heat transfer is calculated with a free convection correlation for horizontal plate with the heated surface facing upward [24–27]:

$$h = \frac{Nu_k}{L} \quad \text{with}$$
$$Nu_L = \begin{cases} 0.54R_a^{0.25} & 10^4 < R_a < 10^7 \\ 0.15R_a^{0.33} & 10^7 < R_a < 10^{11} \end{cases} \tag{14}$$

where Nu is the Nusselt number, L is the characteristic dimension and is equal to the area divided per the perimeter and R_a is the Rayleigh number.

To solve this problem, an implicit-finite difference scheme is chosen. In order to model the sample deformation during vulcanization process, a deforming mesh is considered. At initial time, a simple linear discretization with a constant space step is applied. Based on the mass conservation hypothesis, the mass associated at each volume is assumed constant. Thus, the density variations are represented by volume variations. During whole time course of the treatment, the geometric deformation is only assumed in the thickness direction and a new spatial discretization is recalculated at each iteration:

$$\Delta z_i^t = \frac{\Delta z_i^0 \rho_i^0}{\rho_i^t} \tag{15}$$

4. Results and discussion

In order to validate the numerical model, experimental tests were performed with two different configurations. In a first time, we carried out a heating test with a vulcanized blend. This test aims at the validation of thermal model without the kinetic part and thus enables us to confirm the correct accounting of thermo-physical properties and experimental boundaries (convection, radiation). In a second hand, vulcanization tests were performed. The simulated temperature responses were compared to measurements and the vulcanization profile in the sample thickness was estimated.

4.1. Experimental and simulated thermal responses of a vulcanized plate

For this test, a constant incident radiation at 12.4 kW m^{-2} is maintained during about 300 s (Fig. 9). Initially, the sample is at room temperature, i.e., about 20 °C, as soon as the infrared is applied, the temperature of sample surface rises to reach about

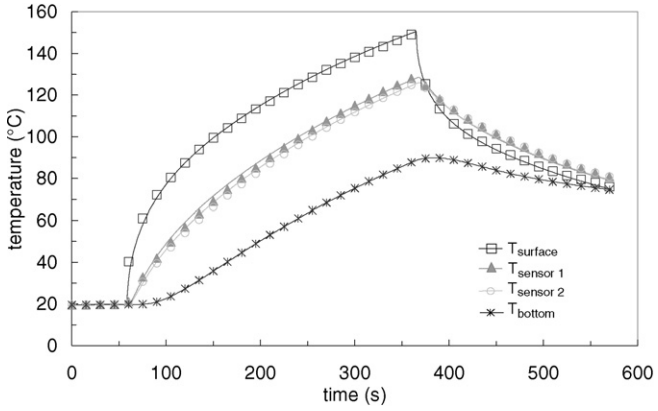

Fig. 9. Heating test (vulcanized sample) with an infrared radiation imposed at 12.4 kW m^{-2}. Comparison between the simulated results (solid lines) and experimental measurements (symbols). Sensor 1 initially at 1.75 mm under surface, sensor 2 at 2 mm.

150 °C. The temperature collected at the sample bottom only increases until 90 °C. Inside the sample, two sensors record the temperature evolutions at a depth of 1.75 mm and at 2 mm. When the infrared radiation is switched off, we note a great decrease in temperature at the surface level caused by the radiative and convective losses (−25 °C in 20 s).

Moreover, in the instance of this pre-vulcanized blend, the dilatation is very small (<0.2 mm), consequently, the problem of thermocouples displacement is negligible.

In comparing the simulated results with those experimentally obtained, a good agreement is observed. During the rise in temperature, the temperature differences between simulation and experimental measurements are relatively low. Indeed, the maximal difference, noticed 2 s after the application of the radiation is less than 8 °C and the deviation does not exceed 2 °C during the heating period. Throughout the cooling, the temperature differences are less than 2 °C for the thermocouples embedded in the sample and are less than 1 °C for the surface temperature. Consequently, this experimental test enables to validate the thermal model in the instance of the heating of vulcanized blend. Moreover, the good agreement observed during the cooling period reveals the correct estimation of boundaries conditions.

4.2. Experimental and simulated thermal responses of a non-vulcanized plate

In the instance of uncured blends, the samples were previously heated at 75 °C inside an air furnace in order to be near industrial conditions, i.e. at the extruder outlet. At the end of the heating, the sample was quickly cooled (quenching in cold water) to stop the vulcanization reaction.

A test realized with an uncured blend and under a heat flux density imposed at 15.8 kW m^{-2} is first presented (Fig. 10). For this vulcanization test, two temperatures were measured inside elastomer sample. Initially, the first thermocouple was positioned at about 0.3 mm under the exposed surface (position of welding center) and the second one was embedded at 2.8 mm.

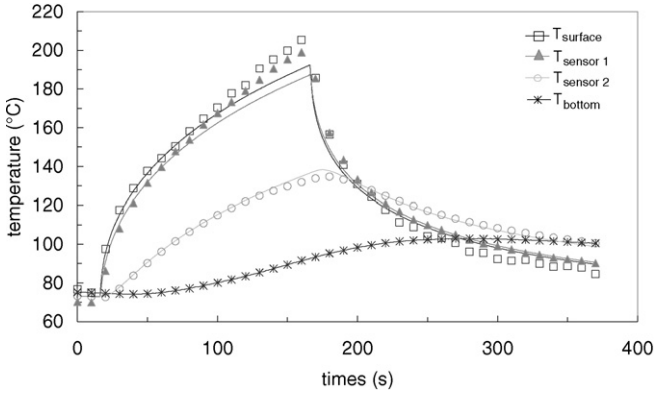

Fig. 10. Vulcanization test (uncured sample) with an infrared radiation imposed at 15.8 kW m^{-2}. Comparison between the simulated results (solid lines) and experimental measurements (symbols). Sensor 1 initially at 0.3 mm under surface, sensor 2 at 2.8 mm.

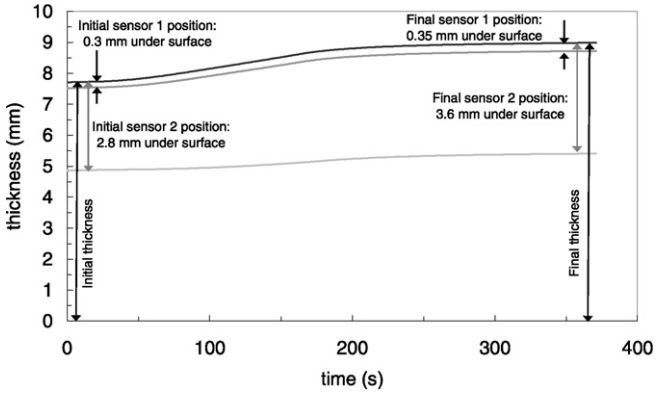

Fig. 11. Thickness evolution and sensors displacement during vulcanization test with a radiation equals to 15.8 kW m^{-2}.

For this test, the infrared radiation, which was applied during about 150 s, generated a quick temperature rise at the sample surface (from about 70 to 210 °C) and, consequently, generated thermal gradients inside the sample (until 120 °C for a thickness of 8.8 mm) caused of the low thermal conduction. During the cooling period, we note a great drop in temperature was recorded (about 60 °C in 20 s for the surface temperature).

The analysis of simulated and experimental data confirms the good representation of thermal phenomena by the numerical model for times less than 100 s. After this time, we note the numerical model underestimates temperatures evolutions. However, the maximum temperatures errors are less than 12.5% at the end of curing period. Moreover, a sensitive analysis showed that several parameters could be causes of errors. Thus, an error of 10% for infrared absorptivity can generate temperature errors more than 7%. Similar errors for other parameters (heat capacity or thermal conductivity) lead to the same consequences. During the cooling period, the simulated temperatures evolutions are in agreement with the ones recorded in the experimental setup. Indeed, the maximal temperature difference is less than 5 °C, which confirms the correct accounting of losses.

In the same time of the temperature response, the numerical model predicts the sample dilatation too during the vulcanization step (Fig. 11). In order to validate the expansion estimated

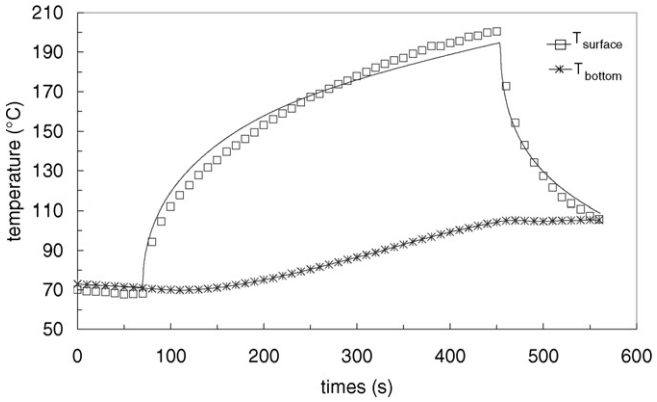

Fig. 12. Vulcanization test (uncured sample) with an infrared radiation imposed at 12.4 kW m^{-2}. Comparison between the simulated results (solid lines) and experimental measurements (symbols).

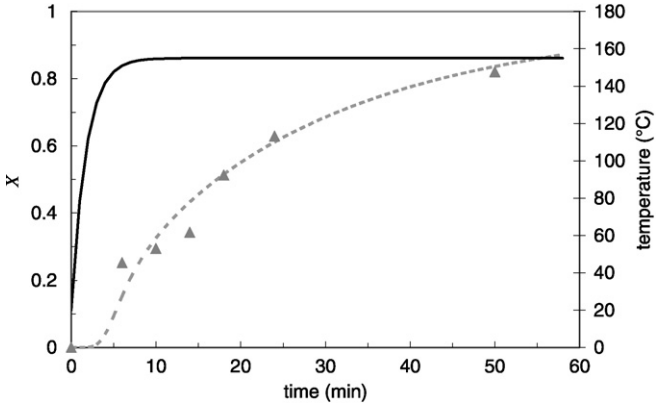

Fig. 13. Vulcanization test in a hot oven. Evolution of samples temperature (solid line) and comparison between the predicted conversion (discontinuous line) and measured conversion (symbols).

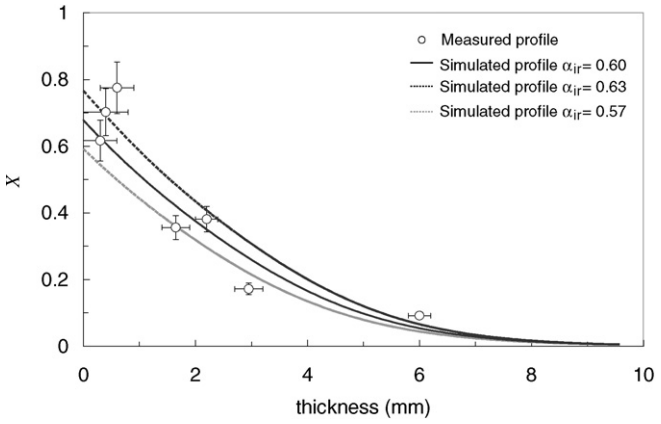

Fig. 14. Final vulcanization profile for test at 12.4 kW m^{-2}: comparison between simulated profile (solid line) and experimental profile (symbols).

by the model, the sample thickness was measured before and after the vulcanization test. Moreover, the sensors' positions were verified a posteriori after the sample cutting.

Initially, the thickness sample was about 7.8 mm and was 8.8 mm at the end of vulcanization test. For this test, the numerical model predicted a final thickness of 9 mm. Regarding the sensors' displacement, a good agreement between model and experimentation is also noticed. Indeed, for the sensor placed just under the surface, its location was measured at 0.35 ± 0.15 mm (sphere diameter error) and the model predicted a sensor location at 0.35 mm. Concerning the other sensor, this one was measured at 3.70 ± 0.15 mm under the surface and the predicted position was at 3.6 mm.

A second test was carried out under an infrared radiation imposed at 12.4 kW m^{-2}. For this test, infrared radiation was applied during about 400 s (Fig. 12). The surface temperature greatly increased until 200 °C whereas the bottom temperature reached only about 100 °C. The observation of Fig. 12 shows there is a good concordance between experimental and simulated data is noted down. Indeed, the differences of temperature do not exceed 7%. About the sample expansion, the final thickness was measured at 9.5 mm and is in agree with the simulation (9.4 mm).

4.3. Validation of vulcanization profile

In order to determine experimentally the states of vulcanization, a calorimetric approach was used. Based on the residual enthalpy measurements and using the formulation below, the average state of vulcanization was estimated [28].

$$X_{\text{end}} = 1 - \frac{\Delta H_{\text{res}}}{\Delta H_{\infty}} \tag{16}$$

To verify the validity of this method, a preliminary test was performed on some small uncured samples (100 mg) vulcanized in a hot oven maintained at 155 °C (convective conditions). The samples were removed from oven at different times (6 to 50 min), these ones were next quickly cooled in cold water to stop the vulcanization reaction. Next, dynamic DSC measurements were conducted. For each test, the DSC runs were performed in a temperature range of 20 to 270 °C at a heating rate of 15 K/min and the residual enthalpy was measured.

The results obtained were next compared with those simulated with a model 0D in convective conditions (Fig. 13) and confirmed the validity of the approach.

In order to determine experimentally the vulcanization profile, this calorimetric approach was next used on the samples previously vulcanized by infrared radiation respectively for a heat flux density imposed at 12.4 kW m^{-2} and at 15.8 kW m^{-2}. Previously, thin sections parallel to the surface were then cut off by a precision saw equipped with an abrasive cut-off wheel (wheel thickness: 0.8 mm). In each section (thickness: 300–500 μm), partially vulcanized matter was next removed and was analyzed calorimetrically

The simulated profile and experimental profile are presented in Figs. 14–15. For each figure, three simulated profiles are plotted in order to show the influence of an error of ±5% for the infrared absorptivity about predicted profiles.

Globally, there is a good agreement between simulated and experimental profiles. Thus, in Fig. 14, for the section corresponding to the position 0.3 mm, the model predicts a state of vulcanization equal to 0.63 ± 0.10. Based on residual enthalpy

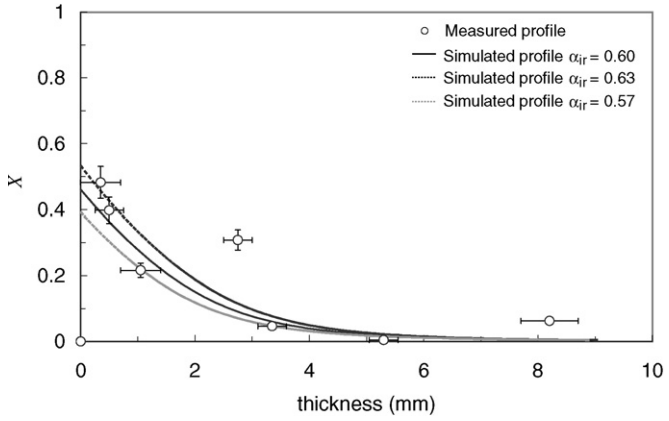

Fig. 15. Final vulcanization profile for test at 15.8 kW m^{-2}: comparison between simulated profile (solid line) and experimental profile (symbols).

results, the degree of vulcanization estimated is included between 0.6 and 0.63 for this section. The error bars represent the errors related to the position of each section (section thickness) and the errors caused by the measurements-uncertainty. However, several differences between simulated and experimental results can be noticed. At 0.6 mm under the exposed surface, the state of vulcanization is experimentally estimated at 0.76–0.79, whereas the model predicts a value of 0.58 ± 0.10. These differences are mainly caused by the blend heterogeneities (bad scattering of components) that consequently generate vulcanization disparities.

5. Conclusion

In this work, superficial elastomer vulcanization by short wave infrared radiation was investigated. The major aim of this study is to predict and validate the depth of vulcanization in the material.

A 1D numerical model enabling the prediction of temperature and conversion rate evolutions in the sample thickness was developed. The modelling was validated by comparison of experimental and simulated test. These tests were performed for two operating conditions (incident radiation: 12 and 15 kW m^{-2}). To validate the predicted vulcanization profile, a methodology based on the cutting up of fine slices in the material thickness coupled with calorimetric analyses was developed. The experimental results allowed the validation of the vulcanization profile in the material.

One of the possible work perspectives is the study of the superficial vulcanization for industrial operating conditions (high infrared input during short treatment times)

Acknowledgements

The authors thank the "Region Bretagne" and the European Social Fund (European Union) for their financial support. The study is supported by "La Société des Polymères Barre Thomas", automotive manufacturer.

References

[1] D. Nichetti, Determination of mechanical properties of silica compounds using a curing kinetic model, Eur. Polym. J. 40 (2004) 2401–2405.
[2] T.-W. Huang, J.-H. Tsai, C.-P. Cherng, J.-K. Chen, Silicone rubber curing by high intensity infrared radiation, in: The Thirteenth International Conference on Thermoelectrics, AIP Conference Proceedings 316, AIP, Kansas City, MO, USA, 1995, pp. 305–308.
[3] L. Véchot, I. Bombard, P. Laurent, J. Lieto, Experimental and modelling study of the radiative curing of a polyester-based coating, Int. J. Therm. Sci. 45 (2006) 86–93.
[4] A. Sadr-Bazaz, R. Granger, J.M. Vergnaud, Calculation of profiles of temperature and state of cure developed within the rubber mass in injection molding process, J. Appl. Polym. Sci. 29 (1984) 955–963.
[5] I.-S. Han, C.-B. Chung, H.-G. Jeong, S.-J. Kang, S.-J. Kim, H.-C. Jung, Optimal cure steps for product quality in a tire curing process, J. Appl. Polym. Sci. 74 (1999) 2063–2071.
[6] M.H.R. Ghoreishy, G. Naderi, Three dimensional finite element modelling of truck tyre curing process in mould, Iranian Polym. J. 14 (2005) 735–743.
[7] S.-O. Pongdhorn, U. Thepsuwan, Prediction of cure level in thick rubber cylinder using finite element analysis, ScienceAsia 28 (2002) 385–391.
[8] T. Behzad, M. Sain, Finite element modelling of polymer curing in natural fiber reinforced composites, Compos. Sci. Technol. 67 (2007) 1666–1673.
[9] V. Kosar, Z. Gomzi, K. Sintic, Modelling and simulation of the continuous power cable processing, Chem. Eng. Process. 46 (2007) 83–88.
[10] V. Kosar, Z. Gomzi, Modelling of the power cable production line, Thermochim. Acta 457 (2007) 70–82.
[11] E. Leroy, J. Dupuy, A. Maazouz, A method of estimating kinetic parameters of thermoset cures: application to a dicyanate ester resin, Macromol. Chem. Phys. 202 (2001) 465–474.
[12] A. Arrillaga, A.M. Zaldua, R.M. Atxurra, A.S. Farid, Techniques used for determining cure kinetics of rubber compounds, Eur. Polym. J. 43 (2007) 4783–4799.
[13] M.A. Kader, C. Nah, Influence of clay on the vulcanization kinetics of fluoroelastomer nanocomposites, Polymer 45 (2004) 2237–2247.
[14] D. Choi, M.A. Kader, B.-H. Cho, Y.-I. Huh, C. Nah, Vulcanization kinetics of nitrile rubber/layered clay nanocomposites, J. Appl. Polym. Sci. 98 (2005) 1688–1696.
[15] S. Mishra, B. Baweja, R. Chandra, Studies on dynamic and static crosslinking of ethylene vinyl acetate and ethylene propylene diene tercopolymer blends, J. Appl. Polym. Sci. 74 (1999) 2756–2763.
[16] J.-L. Bailleul, D. Delaunay, Y. Jarny, Determination of temperature variable properties of composite materials: methodology and experimental results, J. Reinf. Plast. Comp. 15 (1996) 479–496.
[17] S.H. Choug, D.H. Chang, Kinetics of sulfur vulcanization of NR, BR, SBR, and their blends using a rheometer and DSC, J. Appl. Polym. Sci. 61 (1996) 449–454.
[18] R. Ding, A.I. Leonov, A kinetic model for sulfur accelerated vulcanization of a natural rubber compound, J. Appl. Polym. Sci. 61 (1996) 455–463.
[19] M.A. Lopez-Manchado, M. Arroyo, B. Herrero, J. Biagiotti, Vulcanization kinetics of natural rubber-organoclay nanocomposites, J. Appl. Polym. Sci. 89 (2003) 1–15.
[20] P. Salagnac, P. Dutournié, P. Glouannec, Curing of composites by radiation and natural convection in an autoclave, AIChE J. 50 (2004) 3149–3159.
[21] L. Sun, S.-S. Pang, A.M. Sterling, I.I. Negulescu, M.A. Stubblefield, Dynamic modelling of curing process of epoxy prepreg, J. Appl. Polym. Sci. 86 (2002) 1911–1923.
[22] K.J. Dowding, Multi-dimensional estimation of thermal properties and surface heat flux using experimental data and a sequential gradient method, Ph.D. thesis, Michigan State University, USA, 1997.
[23] J. Deans, M. Kögl, The curing of powder coatings using gaseous infrared heaters: an analytical model to assess the process thermal efficiency, Int. J. Therm. Sci. 39 (2000) 762–769.
[24] Y. Bayazitoglu, M.N. Ozisik, Elements of Heat Transfer, McGraw-Hill Book Company, USA, 1988.

[25] J.P. Ploteau, P. Glouannec, H. Noel, Conception of thermoelectric flux meters for infrared radiation measurements in industrial furnaces, Appl. Therm. Eng. 27 (2007) 674–681.
[26] J.R. Ehlert, T.F. Smith, View factors for perpendicular and parallel, rectangular plates, J. Thermophys. Heat Trans. 7 (1993) 173–175.
[27] M. Fishenden, O.A. Saunders, An Introduction to Heat Transfer, Clarendon Press, Oxford, 1950.
[28] F. Heba, M. Mouzali, M.J.M. Abadie, Effect of the crosslinking degree on curing kinetics of an epoxy-acid copolymer system, J. Appl. Polym. Sci. 90 (2003) 2834–2839.